Coexistence of tunable Weyl points and topological nodal lines in ternary transition-metal telluride TaIrTe$_4$

Xiaoqing Zhou,[1,*] Qihang Liu,[2,†] QuanSheng Wu,[3,4] Tom Nummy,[1] Haoxiang Li,[1] Justin Griffith,[1] Stephen Parham,[1]
Justin Waugh,[1] Eve Emmanouilidou,[5] Bing Shen,[5] Oleg V. Yazyev,[3,4] Ni Ni,[5] and Daniel Dessau[1]

[1]*Department of Physics, University of Colorado, Boulder, Colorado 80309, USA*
[2]*Department of Physics, Southern University of Science and Technology of China, Shenzhen 518055, China*
[3]*Institute of Physics, École Polytechnique Fédérale de Lausanne (EPFL), CH-1015 Lausanne, Switzerland*
[4]*National Centre for Computational Design and Discovery of Novel Materials MARVEL, Ecole Polytechnique Fédérale de Lausanne (EPFL),
CH-1015 Lausanne, Switzerland*
[5]*Department of Physics and Astronomy and California NanoSystems Institute, University of California, Los Angeles, California 90095, USA*

We report a combined theoretical and experimental study on TaIrTe$_4$, a potential candidate for a minimal model of type-II Weyl semimetals. Unexpectedly, an intriguing node structure with 12 Weyl points and a pair of nodal lines protected by mirror symmetry was found by first-principles calculations. Some signatures of the complex electronic structure, such as topologically nontrivial band crossings and topologically trivial Fermi arcs, are cross-validated by angle-resolved photoemission spectroscopy. Through external strain, the number of Weyl points can be reduced to a theoretical minimum of four, and the appearance of the nodal lines can be switched between different mirror planes in momentum space. The coexistence of switchable Weyl points and nodal lines establishes transition-metal chalcogenides as a unique test ground for topological state characterization and engineering.

Topological semimetals (SMs) have recently emerged as an active topic due to their exotic physics both in bulk and surface states [1–4], represented by Weyl fermions [1,5–18], Dirac fermions [2,19–22], nodal lines [3,9,23–28], or even quasiparticles without analogous states in the standard model of high-energy physics [29–34]. With the explosion of the discovery of these topological SMs, there arises a natural question of which material should be regarded as a prototype of a given class with simple topological features, such as Bi$_2$Se$_3$ [35] for topological insulators, Na$_3$Bi [22] for Dirac SMs, and CaAs$_3$ for nodal-line SMs [36]. A minimal approach [18] for the Weyl SM is to find the one with a band structure as clean as possible near the Fermi level (E_F) and, more importantly, with the smallest number of Weyl points. Given the complication of the magnetic structure of a time-reversal breaking Weyl SM (such as Mn$_3$Sn [37] and YbMnBi$_2$ [38]), the target of a "hydrogen atom" model for the Weyl SMs has been focused on inversion-breaking SMs with a minimal number of four Weyl points.

Recently, the family of transition-metal chalcogenides MTe$_2$ (M = Mo, W) [6,10–12,15,16] and MM'Te$_4$ (M = Ta, Nb; M' = Ir, Rh) [9,13,14,17,39] has been predicted and experimentally identified as type-II Weyl SMs, with tilted Weyl cones appearing at the boundaries between electron and hole pockets by breaking Lorentz invariance [6,40]. In WTe$_2$ and MoTe$_2$, the underlying Weyl points are clustered together and subject to very subtle lattice constant changes [15,16],

posing difficulties in identifying the number of Weyl points. Furthermore, even the benchmark signature, i.e., the Fermi arcs observed in angle-resolved photoemission spectroscopy (ARPES), could often be "fake evidence" of the Weyl points because of the existence of bulk carrier pockets at the Fermi surface [11,15]. TaIrTe$_4$ has been proposed as the minimal model of a Weyl SM with only four Weyl points well separated in k space above E_F [13], which was supported by a few experimental reports [9,17]. However, in both works [9,17] the spectra near E_F and the Γ point are relatively blurry, imposing challenges to clearly identify the subtle band crossings and surface states. Thus, evidence supporting that the system does not host any other gap closing points is lacking.

To tell if TaIrTe$_4$ is naturally served as a minimal model of a Weyl SM, we use a combination of ARPES and first-principles calculations based on density functional theory (DFT) [41–43] to resolve the electronic structure of TaIrTe$_4$, especially focusing on the details in the center of the Brillouin zone (BZ) where a high momentum resolution is required. In contrast to previous DFT studies [9,17], our theoretical results show that TaIrTe$_4$ hosts a unique combination of 12 Weyl points and two Dirac nodal rings in the BZ. Such a coexistence of different topological features has been theoretically explored [44–47] but has yet to be experimentally confirmed. Our high-momentum-resolution ARPES measurement by 7-eV laser harmonics successfully resolved the details close to the Γ point and found band crossings below E_F as evidence of bulk nodal lines by comparing with our DFT results. We also found apparent surface Fermi arcs that are topologically trivial, indicating the importance of a cross-check between both theory and experiment to confirm the topological features in type-II Weyl
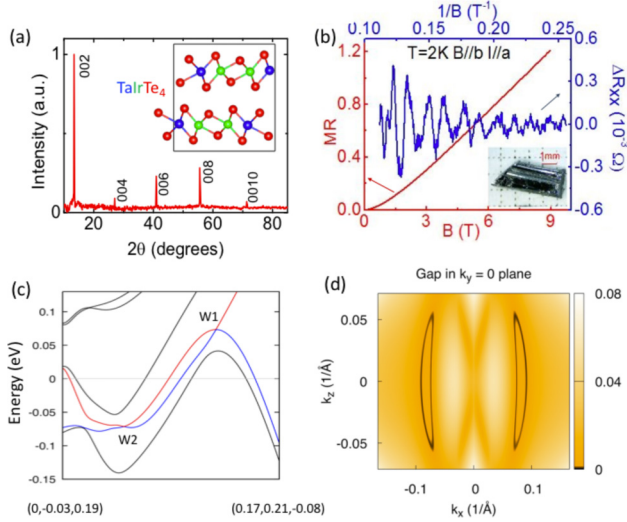
*xiaoqing.zhou@colorado.edu
†liuqh@sustc.edu.cn

FIG. 1. (a) XRD patterns and crystal structure (inset) of TaIrTe$_4$. (b) Magnetoresistance (red) and Shubnikov–de Haas oscillations (blue). Inset: A single crystal of TaIrTe$_4$ against the 1-mm scale. (c) Band structure plotted along the path containing both W1 and W2, in the units of reciprocal lattice vectors. The red and blue lines indicate the conduction and valence band, respectively. (d) Energy gap (in units of eV) in the $k_y = 0$ plane, illustrating two crescent nodal lines.

SMs with complex Fermi surfaces. Our observation thus rules out TaIrTe$_4$ as a minimal model of a Weyl SM, but establishes it as a promising candidate for topological band engineering instead. Notably, applying strain to TaIrTe$_4$ would tune the number of the Weyl points as well as the appearance of the nodal line within different mirror planes in momentum space.

Coexistence of Weyl points and nodal lines in TaIrTe$_4$. The structure of TaIrTe$_4$ could be viewed as a cell-doubling derivative of WTe$_2$, with a $1T'$-type layer structure and Bernal AB stacking. By using single-crystal x-ray diffraction [Fig. 1(a)] we determined the structure as an orthorhombic lattice with $a = 3.80$ Å, $b = 12.47$ Å, and $c = 13.24$ Å, which was used in our DFT calculations [48]. A transport study shows clear quantum oscillations and nonsaturating magnetoresistance [Fig. 1(b)], the latter of which is suggested to be relevant with the existence of Weyl points [49,50]. More details of the synthesis, structural data, and transport properties are shown in Supplemental Material Note 1 [51].

Similar to the type-II Weyl SMs WTe$_2$ and MoTe$_2$, TaIrTe$_4$ has a noncentrosymmetric $Pmn2_1$ (No. 31) space group. This structure contains four symmetry operations: identity, mirror reflection M_x, screw axis operation $\{C_{2z}|(1/2, 0, 1/2)\}$, and a glide reflection operation $\mathcal{M} = \{M_y|(1/2, 0, 1/2)\}$ that transforms (x, y, z) in position space to $(x + a/2, -y, z + c/2)$. Therefore, $\mathcal{M}^2 = -e^{i(k_x + k_z)}$ [52], which means that in the $k_y = 0$ or π plane that is invariant under $\mathcal{M}$, each band has an eigenvalue of $\mathcal{M}$ either $ie^{i(k_x + k_z)/2}$ or $-ie^{i(k_x + k_z)/2}$. In this inversion-breaking system where every band is singly degenerate, the valence and conduction bands may cross each other along a nodal line if they possess opposite $\mathcal{M}$ eigenvalues. Similarly, M_x mirror symmetry can also support nodal-line structures within the $k_x = 0$ or π plane, in the presence of spin-orbit coupling (SOC).

The original goals of replacing Mo/W with Ta and Ir were (1) to realize a material with only four Weyl points, and (2) to extend the separation of Weyl points in momentum space [9,13]. However, our DFT calculations by surveying the band gap over the full BZ show (see Supplemental Material Note 2 for details [51]) that TaIrTe$_4$ has a more complex structure of topological band degeneracies than previously suggested. Besides the four equivalent Weyl points [W1, coordinates $\pm(0.199, 0.071, 0)$ Å^{-1}] located in the $k_z = 0$ plane, in agreement with previous works [9,14,17], we found another eight equivalent type-II Weyl points closer to the Γ point [W2, coordinates $\pm(0.079, 0.021, 0.053)$ Å^{-1}] but off the $k_z = 0$ plane. Figure 1(c) shows the connection between one set of W1 and W2 points in the DFT band structure. W1 is located 74 meV above E_F, for which pump-probe ARPES has confirmed the existence of such unoccupied Weyl cones [9]. On the other hand, the eight W2 Weyl points are 71 meV below E_F, accessible by ARPES but having a smaller k-space separation than that of W1. Interestingly, in TaIrTe$_4$ we also found two nodal lines 67 meV below E_F in the $k_y = 0$ plane in the presence of SOC. Unlike the circlelike shape in other reported nodal-line candidates [9,25,26,36,53], the nodal lines in TaIrTe$_4$ do not surround any high-symmetry points, but form two symmetric, crescent-shaped parts with respect to the Γ point in the BZ [Fig. 1(d)]. This is caused by the large anisotropy between the in-plane x and out-of-plane z directions. As described above, the SOC-robust nodal lines in the $k_y = 0$ plane are protected by the glide reflection operator $\mathcal{M}$, with their nontrivial topology verified by the Berry phase calculations [51].

ARPES measurements of TaIrTe$_4$. Since the difference in surface spectra between the top and bottom surface is too subtle to distinguish by experiments (see Figs. S3 and S4 [51]), we compare our experimental results with the theoretical calculation of the top surface of TaIrTe$_4$. Figure 2(c) shows the Fermi surface observed with ARPES under a synchrotron light of 20-eV photon energy. The first-order features, such as the two side pockets contributed by hole carriers, are generally consistent with the DFT calculations of the bulk band (with a Fermi energy offset of -50 meV) as shown in Fig. 2(a). The four W1 Weyl points fall into these two hole pockets. The E-k dispersion along the Γ-X direction is shown in Fig. 2(e), with overall features similar to those from the previous work of Haubold *et al.* [17]. Nevertheless, the spectra near E_F for both of these "conventional" synchrotron measurements [17] are too blurry to compare with DFT results. To overcome this, we performed measurements in this particular area [black frame in Fig. 2(e)] using 7-eV laser harmonics with markedly improved energy and momentum resolution [54] and perhaps a better matrix element effect (see Supplemental Material Note 3 [51]). The observed spectra revealed many more details than those observed using higher photon energies [as shown in Figs. 2(d) and 2(f)]. In Fig. 2(d), the two side pockets at $k_x = \pm 0.199$ Å^{-1} are not visible in the Fermi map, but the spectra near the center demonstrate several sharp lines representing the Fermi surface. More importantly, the calculated W2 Weyl points as well as the nodal lines are all located in this narrow region [marked in Fig. 2(d)], providing a much better chance to find evidence of these topological features. As shown in Fig. 2(f), the dispersion spectra are also no longer the blob of intensity as in Fig. 2(e).
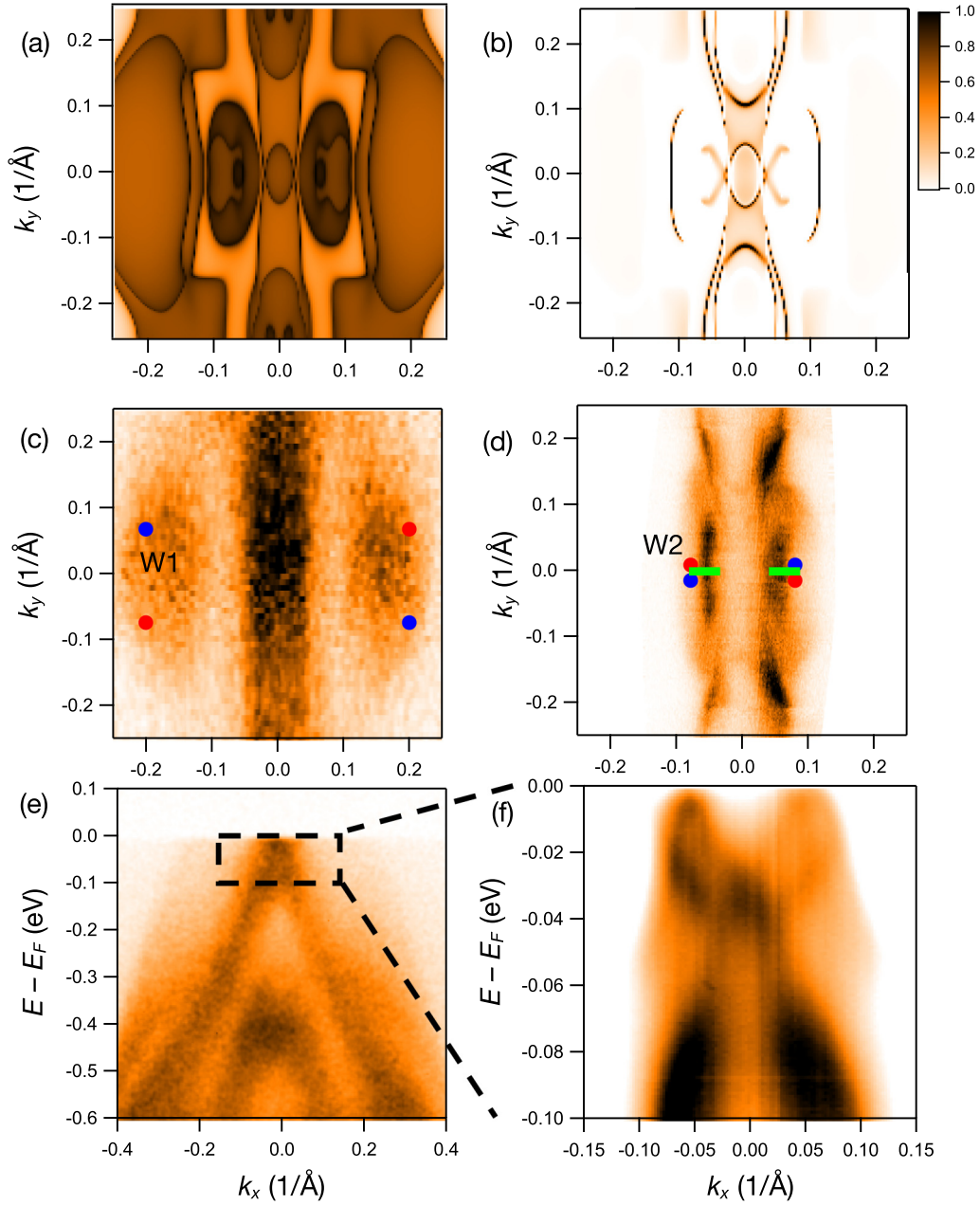
FIG. 2. (a) Momentum-resolved bulk density of states of TaIrTe$_4$ and (b) the corresponding surface-state-only counterpart calculated using DFT at an energy 50 meV below E_F. (c), (d) Experimental ARPES spectra of the Fermi surface taken with (c) 20-eV light, and (d) 7-eV laser harmonics. The calculated Weyl points are marked by red (Chern number $+1$) and blue dots (Chern number -1), whereas the nodal lines projected onto the k_x-k_y plane are represented by the green lines. (e), (f) ARPES spectra along Γ-X for the (e) 28-eV light and (f) 7-eV laser harmonics, respectively.

Specifically, we found two curved branches near the Γ point from E_F to about 40 meV below.

To verify the curved feature in Fig. 2(f), next, we look more closely into surface dispersion by ARPES and connect it to the calculated counterpart. The momentum-resolved local density of states (LDOS) obtained from DFT calculations for the top [001] surface is shown in Fig. 3(a) [the bulk DOS is shown in Fig. S5(a) for comparison [51]]. We first focus on the $k_y = 0$ cut, where both W2 Weyl points and nodal lines could be resolved. Compared with the bulk state, the surface LDOS from Fig. 3(a) suggests that as the surface band merges into the

bulk band, only the left band-crossing point at $k_x = 0.07\,\text{Å}^{-1}$ is clearly presented. Our ARPES observation fits the calculated surface dispersion very well [as shown in Fig. 3(b)], with only the bands on the left of the first crossing point of the nodal line visible. In contrast, the W2 Weyl points overlap with the second band-crossing points, and so their signatures are likely invisible under 7-eV laser harmonics. Overall, such a good agreement between DFT and ARPES confirms that TaIrTe$_4$ is not a "hydrogen atom" model for Weyl semimetals; instead, it hosts a zero- plus one-dimensional (0D Weyl points + 1D Dirac nodal lines) combination of the nodal surface.
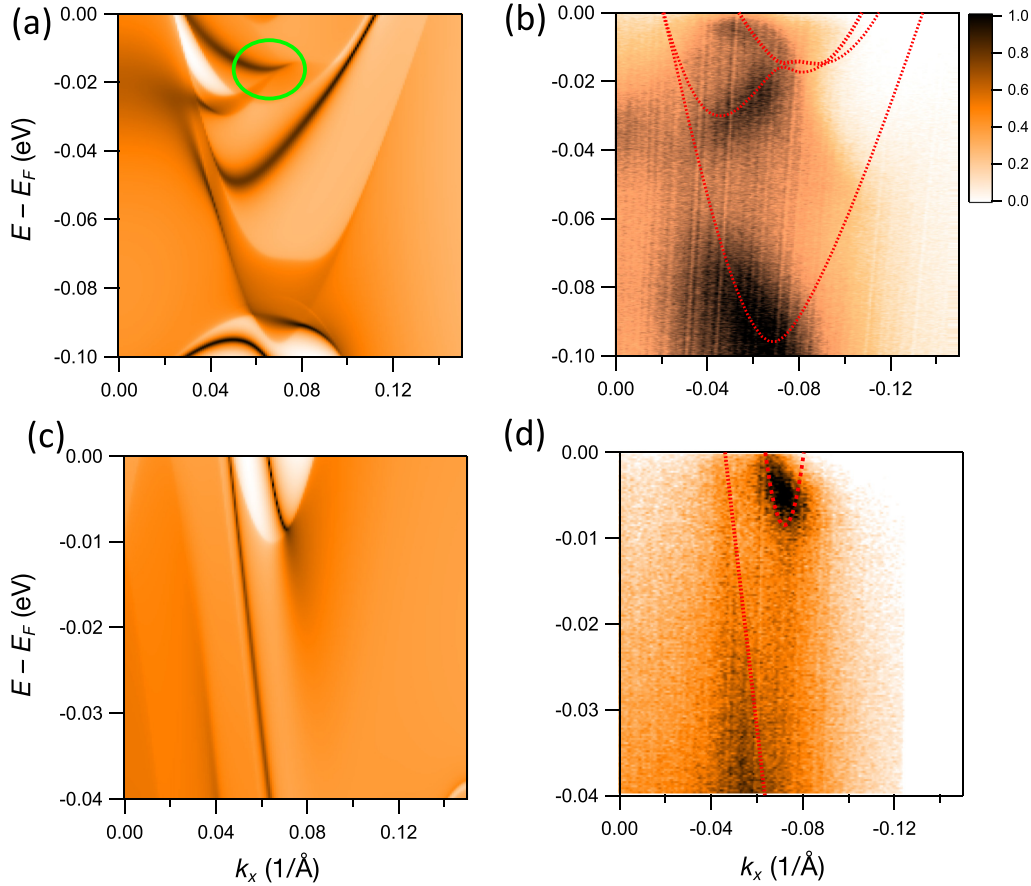
FIG. 3. (a) Momentum-resolved local density of states of TaIrTe$_4$ for the [001] surface at $k_y = 0$ obtained from DFT calculations, to be compared with (b) experimental ARPES spectra taken with 7-eV laser harmonics. (c), (d) Same as (a), (b) but for the cut at $k_y = 0.25\,\text{Å}^{-1}$. The red dashed lines in (b) and (d) are guides to the eye from DFT results.

In general, a type-II Weyl SM hosts a relatively complicated Fermi surface in which some topologically trivial surface states could emerge from the bulk continuum, behaving as Fermi arcs. Such trivial Fermi arcs happen in both MoTe$_2$ and WTe$_2$ [10,15], and also in TaIrTe$_4$. For example, Figs. 3(c) and 3(d) show the theoretical and experimental dispersion spectra below E_F at the $k_y = 0.25\,\text{Å}^{-1}$ cut. Comparing with Fig. 3(c) [see also Fig. S5(b) for the bulk state [51]], we find that the parabolic electron pocket in the bulk LDOS [Fig. S3(b)] is truncated in the surface LDOS [Fig. 3(c)], indicating that only the left part of the surface state emerges from the bulk, forming a trivial Fermi arc. The ARPES spectra shown in Fig. 3(d) show good agreement with the theoretical prediction. Particularly notable in the spectra is a dispersion that has $k_x = -0.065\,\text{Å}^{-1}$ and terminates at $-8\,\text{meV}$, which resembles a half of a parabolic band and thus seems as a Fermi arc. However, from the verification by DFT calculations we conclude that this appearance is merely the result of a surface band merging into the relatively invisible bulk band at this photon energy. Thus in Weyl SMs with relatively complex Fermi surfaces, the experimentally observed Fermi arc cannot serve as direct evidence of the existence of a Weyl point or the underlying topological characters [15].

For nodal-line SMs, it is predicted that a "drumhead" surface state will form along the nodal-line band-crossing

points. However, although the nodal lines protected by a specific crystal symmetry indeed lead to a nontrivial Berry phase (e.g., π in TaIrTe$_4$), such a Berry phase is not sufficient to form a topologically protected surface state. In other words, the expected "drumhead" surface state could be adiabatically deformed into the bulk continuum without any symmetry breaking. A similar situation appears in Dirac SMs where the Fermi arcs on the surface are not topologically protected and can be continuously deformed into a case of a topological or normal insulator [55]. Therefore, we do not expect to verify the existence of nodal lines in TaIrTe$_4$ through surface states.

Tuning the topological band degeneracies by volume change. Modifying the number of Weyl points by external "knobs," such as strain, is of practical importance as it may allow one to achieve a simple Fermi surface with only a minimum number of Weyl nodes, and thus could offer a clearer signature of various topological properties such as the chiral anomaly [56]. On the other hand, a nodal line robust to SOC requires specific mirror symmetries (M_x and $\mathcal{M}$) as mentioned above, and thus appears only within the $k_x, k_y = 0$ or π mirror plane. Therefore, the location of the nodal lines could also be tuned by changing the lattice parameters. Here, we studied the topological transition of bulk TaIrTe$_4$ in regards to a volume change within the range of $\alpha = \frac{V - V_0}{V} = \pm 15\%$, where V_0 is the volume under ambient pressure. Not surprisingly, the
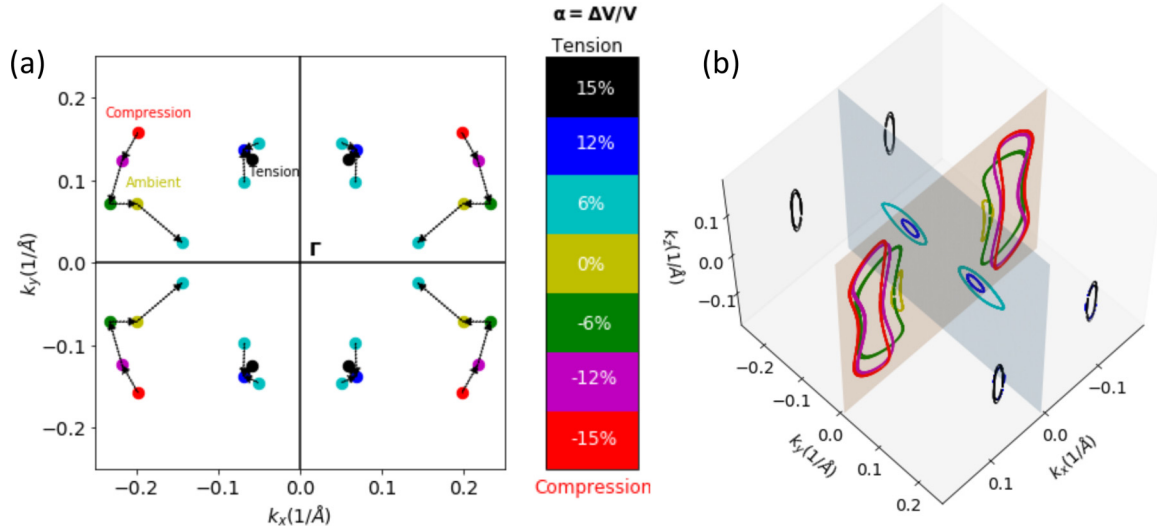
FIG. 4. (a) Evolution of Weyl points W1 upon volume change $\Delta V / V$ from -15% to 15%. (b) Nodal lines switching from the $k_y = 0$ mirror plane (red shade) to $k_x = 0$ (blue shade) and $k_y = \pi$ mirror planes with a volume increase.

majority of change occurs along the c axis, which governs the interplane coupling strength. We first focus on the Weyl points. Given the C_{2z} rotational symmetry and time-reversal symmetry T, the combined symmetry $C_{2z}T$ transforms (k_x, k_y, k_z) to $(k_x, k_y, -k_z)$ and maintains the chirality of the Weyl point. Therefore, besides the ordinary W2 points with arbitrary (k_x, k_y, k_z), the Weyl points could also be pinned at the $k_z = 0$ plane, forming a W1 class, which in general cannot transform to W2 points because of the charge conversion. Within the range of α considered, there are always some W1 Weyl points within the $k_z = 0$ plane [14] [see Fig. 4(a)], but with an intriguing transformation. The "original" four W1 Weyl points appear to be quite robust and persist until $\alpha > 6\%$. On the other hand, at $\alpha = 6\%$, $4+4$ extra W1 points 34 and 58 meV below E_F emerge elsewhere and evolve into four at $\alpha > 6\%$. Eight W2 Weyl points below E_F emerge at $\alpha = -12\%$, approach the k_x-k_y plane as the volume increases, and annihilate at $\alpha = 6\%$ (see Supplemental Material Note 4 [51]). Therefore, a relatively simple node structure with a minimal number of Weyl points can be obtained with $6\% \leqslant \alpha \leqslant 15\%$.

Whereas the topology of nodal lines remains unchanged under compression, it evolves dramatically with volume expansion, as shown in Fig. 4(b). As nodal lines robust to SOC require specific mirror symmetries (M_x and $\mathcal{M}$), they appear only within the $k_x, k_y = 0$ or π mirror plane. The two crescent nodal lines within the $k_y = 0$ plane disappear at $\alpha = 6\%$, while two nodal lines within the $k_x = 0$ plane, protected by M_x, are created. Such a nodal-line transition has an interesting implication for device physics as the corresponding surface state can be switched between different crystal faces. The nodal lines within the $k_x = 0$ plane still exist for $\alpha = 12\%$ but disappear at $\alpha = 15\%$. Moreover, a new pair of nodal lines within in the $k_y = \pi$ plane appear in both cases. In the case $\alpha = 12\%$ and 15%, the node structure is composed of four Weyl points and nodal lines with energies close to E_F and an energy separation between the Weyl points and nodal lines of about 15 meV. Therefore, we could expect a relatively simple Fermi surface for examining either the Weyl or nodal-line topological

features by tuning the doping levels in the same material. Volume expansion might be achieved through intercalation chemistry [57,58], which has been widely used in transition-metal chalcogenides to tune the c-axis lattice constant.

Furthermore, we stress that the coexistence of topological order morphology we reported here might not be limited to TaIrTe$_4$ alone. Recently, it was found [59] that the topological orders are ubiquitous among the family of MX_2 or $MM'X_4$ (M, M' = transition metals, X = S, Se, or Te), the evolution of which is largely determined by the interlayer coupling, i.e., c-axis lattice constant [14]. While we made the accidental discovery of the coexistence of two topological orders as well as the switching of Weyl points and nodal lines in TaIrTe$_4$, it remains an open question whether a similar, or even a simpler and more accessible, topological order transformation can be discovered in others among this family, especially those with similar structures such as WTe$_2$. As demonstrated by this work, a definite answer can only be reached by a thorough search in the momentum space with careful and precise exploration.

In conclusion, by using a combination of ARPES measurements and DFT calculations we find that TaIrTe$_4$ possesses a complex node structure with 12 Weyl points and two crescent nodal lines in the BZ, as opposed to a minimal model of a Weyl SM. The delicate entanglement between conduction and valence bands also offers the possibility to tune the topology of the Weyl points and nodal lines by moderate strain. By observing topologically trivial Fermi arcs at surface, this work also highlights the importance of the cross-validation between both theory and experiment to confirm the topological features in such type-II Weyl SMs.

[1] X. Wan, A. M. Turner, A. Vishwanath, and S. Y. Savrasov, Phys. Rev. B **83**, 205101 (2011).

[2] Z. Wang, Y. Sun, X.-Q. Chen, C. Franchini, G. Xu, H. Weng, X. Dai, and Z. Fang, Phys. Rev. B **85**, 195320 (2012).

[3] A. A. Burkov, M. D. Hook, and L. Balents, Phys. Rev. B **84**, 235126 (2011).

[4] H. Weng, X. Dai, and Z. Fang, J. Phys.: Condens. Matter **28**, 303001 (2016).

[5] B. Q. Lv, H. M. Weng, B. B. Fu, X. P. Wang, H. Miao, J. Ma, P. Richard, X. C. Huang, L. X. Zhao, G. F. Chen, Z. Fang, X. Dai, T. Qian, and H. Ding, Phys. Rev. X **5**, 031013 (2015).

[6] A. A. Soluyanov, D. Gresch, Z. Wang, Q. Wu, M. Troyer, X. Dai, and B. A. Bernevig, Nature (London) **527**, 495 (2015).

[7] H. Weng, C. Fang, Z. Fang, B. A. Bernevig, and X. Dai, Phys. Rev. X **5**, 011029 (2015).

[8] S.-Y. Xu, I. Belopolski, N. Alidoust, M. Neupane, G. Bian, C. Zhang, R. Sankar, G. Chang, Z. Yuan, C.-C. Lee, S.-M. Huang, H. Zheng, J. Ma, D. S. Sanchez, B. Wang, A. Bansil, F. Chou, P. P. Shibayev, H. Lin, S. Jia, and M. Z. Hasan, Science **349**, 613 (2015).

[9] I. Belopolski, P. Yu, D. S. Sanchez, Y. Ishida, T.-R. Chang, S. S. Zhang, S.-Y. Xu, H. Zheng, G. Chang, G. Bian, H.-T. Jeng, T. Kondo, H. Lin, Z. Liu, S. Shin, and M. Zahid Hasan, Nat. Commun. **8**, 942 (2017).

[10] F. Y. Bruno, A. Tamai, Q. S. Wu, I. Cucchi, C. Barreteau, A. de la Torre, S. McKeown Walker, S. Riccò, Z. Wang, T. K. Kim, M. Hoesch, M. Shi, N. C. Plumb, E. Giannini, A. A. Soluyanov, and F. Baumberger, Phys. Rev. B **94**, 121112(R) (2016).

[11] K. Deng, G. Wan, P. Deng, K. Zhang, S. Ding, E. Wang, M. Yan, H. Huang, H. Zhang, Z. Xu, J. Denlinger, A. Fedorov, H. Yang, W. Duan, H. Yao, Y. Wu, S. Fan, H. Zhang, X. Chen, and S. Zhou, Nat. Phys. **12**, 1105 (2016).

[12] L. Huang, T. M. McCormick, M. Ochi, Z. Zhao, M.-T. Suzuki, R. Arita, Y. Wu, D. Mou, H. Cao, J. Yan, N. Trivedi, and A. Kaminski, Nat. Mater. **15**, 1155 (2016).

[13] K. Koepernik, D. Kasinathan, D. V. Efremov, S. Khim, S. Borisenko, B. Büchner, and J. van den Brink, Phys. Rev. B **93**, 201101 (2016).

[14] J. Liu, H. Wang, C. Fang, L. Fu, and X. Qian, Nano Lett. **17**, 467 (2017).

[15] A. Tamai, Q. S. Wu, I. Cucchi, F. Y. Bruno, S. Riccò, T. K. Kim, M. Hoesch, C. Barreteau, E. Giannini, C. Besnard, A. A. Soluyanov, and F. Baumberger, Phys. Rev. X **6**, 031021 (2016).

[16] Z. Wang, D. Gresch, A. A. Soluyanov, W. Xie, S. Kushwaha, X. Dai, M. Troyer, R. J. Cava, and B. A. Bernevig, Phys. Rev. Lett. **117**, 056805 (2016).

[17] E. Haubold, K. Koepernik, D. Efremov, S. Khim, A. Fedorov, Y. Kushnirenko, J. van den Brink, S. Wurmehl, B. Büchner, T. K. Kim, M. Hoesch, K. Sumida, K. Taguchi, T. Yoshikawa, A. Kimura, T. Okuda, and S. V. Borisenko, Phys. Rev. B **95**, 241108 (2017).

[18] T. M. McCormick, I. Kimchi, and N. Trivedi, Phys. Rev. B **95**, 075133 (2017).

[19] S. M. Young, S. Zaheer, J. C. Y. Teo, C. L. Kane, E. J. Mele, and A. M. Rappe, Phys. Rev. Lett. **108**, 140405 (2012).

[20] Z. Wang, H. Weng, Q. Wu, X. Dai, and Z. Fang, Phys. Rev. B **88**, 125427 (2013).

[21] Z. K. Liu, J. Jiang, B. Zhou, Z. J. Wang, Y. Zhang, H. M. Weng, D. Prabhakaran, S. K. Mo, H. Peng, P. Dudin, T. Kim, M. Hoesch, Z. Fang, X. Dai, Z. X. Shen, D. L. Feng, Z. Hussain, and Y. L. Chen, Nat. Mater. **13**, 677 (2014).

[22] Z. K. Liu, B. Zhou, Y. Zhang, Z. J. Wang, H. M. Weng, D. Prabhakaran, S. K. Mo, Z. X. Shen, Z. Fang, X. Dai, Z. Hussain, and Y. L. Chen, Science **343**, 864 (2014).

[23] Y. Chen, Y.-M. Lu, and H.-Y. Kee, Nat. Commun. **6**, 6593 (2015).

[24] C. Fang, Y. Chen, H.-Y. Kee, and L. Fu, Phys. Rev. B **92**, 081201 (2015).

[25] H. Weng, Y. Liang, Q. Xu, R. Yu, Z. Fang, X. Dai, and Y. Kawazoe, Phys. Rev. B **92**, 045108 (2015).

[26] G. Bian, T.-R. Chang, R. Sankar, S.-Y. Xu, H. Zheng, T. Neupert, C.-K. Chiu, S.-M. Huang, G. Chang, I. Belopolski, D. S. Sanchez, M. Neupane, N. Alidoust, C. Liu, B. Wang, C.-C. Lee, H.-T. Jeng, C. Zhang, Z. Yuan, S. Jia *et al.*, Nat. Commun. **7**, 10556 (2016).

[27] T. Bzdusek, Q. Wu, A. Rüegg, M. Sigrist, and A. A. Soluyanov, Nature (London) **538**, 75 (2016).

[28] E. Emmanouilidou, B. Shen, X. Deng, T.-R. Chang, A. Shi, G. Kotliar, S.-Y. Xu, and N. Ni, Phys. Rev. B **95**, 245113 (2017).

[29] B. Bradlyn, J. Cano, Z. Wang, M. G. Vergniory, C. Felser, R. J. Cava, and B. A. Bernevig, Science **353**, 5037 (2016).

[30] H. Weng, C. Fang, Z. Fang, and X. Dai, Phys. Rev. B **93**, 241202 (2016).

[31] B. J. Wieder, Y. Kim, A. M. Rappe, and C. L. Kane, Phys. Rev. Lett. **116**, 186402 (2016).

[32] Z. Zhu, G. W. Winkler, Q. S. Wu, J. Li, and A. A. Soluyanov, Phys. Rev. X **6**, 031003 (2016).

[33] Q. Liu and A. Zunger, Phys. Rev. X **7**, 021019 (2017).

[34] B. Q. Lv, Z. L. Feng, Q. N. Xu, X. Gao, J. Z. Ma, L. Y. Kong, P. Richard, Y. B. Huang, V. N. Strocov, C. Fang, H. M. Weng, Y. G. Shi, T. Qian, and H. Ding, Nature (London) **546**, 627 (2017).

[35] D. Hsieh, Y. Xia, D. Qian, L. Wray, J. H. Dil, F. Meier, J. Osterwalder, L. Patthey, J. G. Checkelsky, N. P. Ong, A. V. Fedorov, H. Lin, A. Bansil, D. Grauer, Y. S. Hor, R. J. Cava, and M. Z. Hasan, Nature (London) **460**, 1101 (2009).

[36] Y. Quan, Z. P. Yin, and W. E. Pickett, Phys. Rev. Lett. **118**, 176402 (2017).

[37] K. Kuroda, T. Tomita, M. T. Suzuki, C. Bareille, A. A. Nugroho, P. Goswami, M. Ochi, M. Ikhlas, M. Nakayama, S. Akebi, R. Noguchi, R. Ishii, N. Inami, K. Ono, H. Kumigashira, A. Varykhalov, T. Muro, T. Koretsune, R. Arita, S. Shin *et al.*, Nat. Mater. **16**, 1090 (2017).

[38] S. Borisenko, D. Evtushinsky, Q. Gibson, A. Yaresko, T. Kim, M. N. Ali, B. Buechner, M. Hoesch, and R. J. Cava, arXiv:1507.04847.

[39] L. Li, H.-H. Xie, J.-S. Zhao, X.-X. Liu, J.-B. Deng, X.-R. Hu, and X.-M. Tao, Phys. Rev. B **96**, 024106 (2017).

[40] Y. Xu, F. Zhang, and C. Zhang, Phys. Rev. Lett. **115**, 265304 (2015).

[41] G. Kresse and J. Furthmüller, Comput. Mater. Sci. **6**, 15 (1996).

[42] J. P. Perdew, K. Burke, and M. Ernzerhof, Phys. Rev. Lett. **77**, 3865 (1996).

[43] G. Kresse and D. Joubert, Phys. Rev. B **59**, 1758 (1999).

[44] K.-H. Ahn, W. E. Pickett, and K. W. Lee, arXiv:1803.08172.

[45] H. Gao, Y. Kim, J. W. F. Venderbos, C. L. Kane, E. J. Mele, A. M. Rappe, and W. Ren, arXiv:1802.04815.

[46] H. Zhang, Y. Xie, Z. Zhang, C. Zhong, Y. Li, Z. Chen, and Y. Chen, J. Phys. Chem. Lett. **8**, 1707 (2017).

[47] J.-P. Sun, D. Zhang, and K. Chang, Phys. Rev. B **96**, 045121 (2017).

[48] We also calculated the slightly different structure used in Refs. [9,17] and found similar results, as shown in Supplementam Material Note 2.

[49] T. Liang, Q. Gibson, M. N. Ali, M. Liu, R. J. Cava, and N. P. Ong, Nat. Mater. **14**, 280 (2015).

[50] S. Khim, K. Koepernik, D. V. Efremov, J. Klotz, T. Förster, J. Wosnitza, M. I. Sturza, S. Wurmehl, C. Hess, J. van den Brink, and B. Büchner, Phys. Rev. B **94**, 165145 (2016).

[51] See Supplemental Material at http://link.aps.org/supplemental/10.1103/PhysRevB.97.241102 for Refs. [60–64] and further details concerning the experiments and calculations.

[52] $\hat{\mathcal{M}}$ transforms (x,y,z) to $(x+a,y,z+c)$, and in the presence of SOC with the antiunitary operator T behaving as $T^2 = -1$, rotates spin by 2π, leading to a factor of -1 for a spin-1/2 system.

[53] R. Yu, H. Weng, Z. Fang, X. Dai, and X. Hu, Phys. Rev. Lett. **115**, 036807 (2015).

[54] J. D. Koralek, J. F. Douglas, N. C. Plumb, Z. Sun, A. V. Federov, M. M. Murnane, H. C. Kapteyn, S. T. Cundiff, Y. Aiura, K. Oka, H. Eisaki, and D. S. Dessau, Phys. Rev. Lett. **96**, 017005 (2006).

[55] M. Kargarian, M. Randeria, and Y.-M. Lu, Proc. Natl. Acad. Sci. U.S.A. **113**, 8648 (2016).

[56] J. Xiong, S. K. Kushwaha, T. Liang, J. W. Krizan, M. Hirschberger, W. Wang, R. J. Cava, and N. P. Ong, Science **350**, 413 (2015).

[57] F. R. Gamble, J. H. Osiecki, M. Cais, R. Pisharody, F. J. DiSalvo, and T. H. Geballe, Science **174**, 493 (1971).

[58] Y. Jung, Y. Zhou, and J. J. Cha, Inorg. Chem. Front. **3**, 452 (2016).

[59] M. S. Bahramy, O. J. Clark, B. J. Yang, J. Feng, L. Bawden, J. M. Riley, I. Marković, F. Mazzola, V. Sunko, D. Biswas, S. P. Cooil, M. Jorge, J. W. Wells, M. Leandersson, T. Balasubramanian, J. Fujii, I. Vobornik, J. E. Rault, T. K. Kim, M. Hoesch *et al.*, Nat. Mater. **17**, 21 (2017).

[60] P. C. Canfield and Z. Fisk, Philos. Mag. B **65**, 1117 (1992).

[61] I. Souza, N. Marzari, and D. Vanderbilt, Phys. Rev. B **65**, 035109 (2001).

[62] A. A. Mostofi, J. R. Yates, G. Pizzi, Y.-S. Lee, I. Souza, D. Vanderbilt, and N. Marzari, Comput. Phys. Commun. **185**, 2309 (2014).

[63] M. P. L. Sancho, J. M. L. Sancho, J. M. L. Sancho, and J. Rubio, J. Phys. F **15**, 851 (1985).

[64] Q. Wu, S. Zhang, H.-F. Song, M. Troyer, and A. A. Soluyanov, Comput. Phys. Commun. **224**, 405 (2018).